Mathematical and Analog Modeling of Lava Dome Growth

Amy Shen

1 Introduction

Lava domes are masses of solid rock that are formed when molten lava erupts slowly from a vent. The traveling distance and speed of a lava flow depends on the effusion rate, the fluidity of the lava, the volume erupted, the channel geometry, and the obstructions in the path of flow. Between 1980 and 1986, Mount St. Helens built a lava dome approximately 1,000 feet high and 3,500 feet in diameter. The burning, crushing, and other effects associated with lava flows can cause extensive damage. As lava domes spread slowly, they typically do not endanger human life, however, they can destroy permanent structures.

Lava domes are the simplest type of lava flow. If the lava is sufficently viscous, it will pile up above the vent to form a dome. Usually such lava is composed of high-silica andesite and dacite. To minimize the damage of lava flows to human resources, numerous studies have been performed over the past 100 years. The central goal of these studies is to predict flow growth and the eruption state. Due to the difficulty of obtaining field measurements, labarotary simulation provides a good alternative approach to obtaining data. As lava often shows a non-Newtonian behavior with a finite yield stress, appropriate materials for these laboratory studies should posses such rheological characteristics. For isothermal studies, slurries, consisting, for example, of water and kaoline, have been used with some success. However, more realistically, the role of cooling at the lava surface exerts an important influence on flow structure and morphology. Griffiths, Fink and other resarchers[5−9] studied the morphology of the dome surface in recent years, and in so doing, took the surface cooling and the solidification of the lava into account. In particular, experiments and a scaling analysis that yielded approximate radius and height profiles evolving with time were performed.[2,7,8]

The work presented here is based on the hypothesis that the flowing lava can be modeled as a Bingham fluid. Following some theoretical preliminaries, an isothermal model is presented and a thin layer theory is applied. Analytical and experimental results are then compared. The results from the isothermal model proposed here fit quite well with our experimental data. Later, the surface cooling of the flow is taken into account through a depth averaged temperature field. Analytical and numerical results show some qualitatively different flow features compared to the isothermal case. Further, spreading of kaoline and PEG600 wax mixture, which is a slurry that has a highly temperature dependent viscosity and yield stress under cold water is studied in the laboratory.

2 Theoretical Preliminaries

We consider a lava flow that occupies a region $\mathcal{R}$ of three-dimensional Euclidiean space. The basic variables of the theory are

ϱ	mass density,
$\boldsymbol{v}$	particle velocity,
$\boldsymbol{T}$	Cauchy stress tensor,
$\boldsymbol{g}$	gravitational acceleration,
ε	specific internal energy,
$\boldsymbol{q}$	heat flux vector,
η	specific entropy,
θ	(absolute) temperature.

We assume that the medium is incompressible, so that

$$\operatorname{div}\boldsymbol{v} = 0; \tag{1}$$

this being the case, it is useful to introduce the extra stress $\boldsymbol{S}$ and the pressure, defined so that

$$\boldsymbol{S} = \boldsymbol{T} + p\boldsymbol{1}, \qquad p = -\tfrac{1}{3}\operatorname{tr}\boldsymbol{T}. \tag{2}$$

Clearly, $\boldsymbol{S}$, so defined, is traceless.

The basic variables satisfy the field equations

$$\left.\begin{aligned} \varrho\dot{\boldsymbol{v}} &= -\operatorname{grad}p + \operatorname{div}\boldsymbol{S} + \varrho\boldsymbol{g}, \\ \boldsymbol{S} &= \boldsymbol{S}^{\top}, \\ \varrho\dot{\varepsilon} = \boldsymbol{S}\cdot\boldsymbol{D} - \operatorname{div}\boldsymbol{q} \qquad & \big(\boldsymbol{D} = \tfrac{1}{2}(\operatorname{grad}\boldsymbol{v} + \operatorname{grad}\boldsymbol{v}^{\top})\big), \end{aligned}\right\} \tag{3}$$

which express linear momentum balance, angular momentum balance, and energy balance, as well as the field inequality

$$\varrho\dot{\eta} \geq -\operatorname{div}\left(\frac{\boldsymbol{q}}{\theta}\right), \tag{4}$$

which expresses entropy imbalance. Note that $\dot{f}$ denotes the material time-rate of a field f. If we introduce the specific free energy

$$\psi = \varepsilon - \theta\eta, \tag{5}$$

the entropy inequality (4) can be rewritten in the form

$$\varrho(\dot{\psi} + \eta\dot{\theta}) - \boldsymbol{S}\cdot\boldsymbol{D} + \frac{1}{\theta}\boldsymbol{q}\cdot\operatorname{grad}\theta \leq 0. \tag{6}$$

We assume that ψ and η are determined constitutively via the relations

$$\psi = \hat{\psi}(\theta) = c\theta(1 - \log\frac{\theta}{\theta_0}) \qquad \text{and} \qquad \eta = \hat{\eta}(\theta) = c\log\frac{\theta}{\theta_0}, \tag{7}$$

where $c = \text{constant} > 0$ denotes the specific heat and $\theta_0 > 0$ is a given base temperature. Granted these assumptions, a simple calculation shows that

$$\dot{\psi} + \eta\dot{\theta} = 0, \tag{8}$$

whereby the inequality (6) reduces to

$$-\boldsymbol{S}\cdot\boldsymbol{D} + \frac{1}{\theta}\boldsymbol{q}\cdot\operatorname{grad}\theta \leq 0. \tag{9}$$

Next, we suppose that the strain-rate $\boldsymbol{D}$ and the dissipative contribution $\boldsymbol{S}$ to the stress obey a Bingham thermo-visco-plastic relation

$$\boldsymbol{D} = \begin{cases} \boldsymbol{0} & \text{if } |\boldsymbol{S}| < s_y(\theta), \\ \dfrac{1}{\mu(\theta)}\big(|\boldsymbol{S}| - s_y(\theta)\big)\boldsymbol{S} & \text{if } |\boldsymbol{S}| > s_y(\theta), \end{cases} \tag{10}$$

with $\mu(\theta) > 0$ the reciprocal mobility and $s_y(\theta) > 0$ the yield stress, and, further, that the heat conduction is of Fourier type, so that

$$\boldsymbol{q} = -\kappa\operatorname{grad}\theta, \tag{11}$$

with $\kappa = \text{constant} > 0$ the thermal conductivity. With these assumptions, it transpires that

$$\boldsymbol{S}\cdot\boldsymbol{D} - \frac{1}{\theta}\boldsymbol{q}\cdot\operatorname{grad}\theta = \left.\begin{cases} \dfrac{1}{\theta}\kappa|\operatorname{grad}\theta|^2 & \text{if } |\boldsymbol{S}| < s_y(\theta), \\ \dfrac{1}{\mu(\theta)}\big(|\boldsymbol{S}| - s_y(\theta)\big)|\boldsymbol{S}|^2 + \dfrac{1}{\theta}\kappa|\operatorname{grad}\theta|^2 & \text{if } |\boldsymbol{S}| > s_y(\theta) \end{cases}\right\} \geq 0, \tag{12}$$

from which we conclude that the reduced entropy inequality (9) is guaranteed to hold in all processes.

For $|\boldsymbol{S}| > s_y(\theta)$, the choice (10) implies that

$$\boldsymbol{S} = \big(\mu(\theta) + \frac{s_y(\theta)}{|\boldsymbol{D}|}\big)\boldsymbol{D}. \tag{13}$$

Hence, provided $|\boldsymbol{S}| > s_y(\theta)$, the linear momentum balance $(3)_1$ takes the form

$$\varrho\dot{\boldsymbol{v}} = -\operatorname{grad}p + \varrho\boldsymbol{g} + \operatorname{div}\Big(\big(\mu(\theta) + \frac{s_y(\theta)}{|\boldsymbol{D}|}\big)\boldsymbol{D}\Big) \tag{14}$$

and the angular momentum balance $(3)_2$ is satisfied trivially. Further, from the definition (5) of ψ and the relations (7) determining ψ and η in terms of θ, we have that

$$\varepsilon = c\theta, \tag{15}$$

whence, bearing in mind (11) and (13), the energy balance $(3)_3$ simplifies to

$$\varrho c\dot{\theta} = \kappa\operatorname{div}(\operatorname{grad}\theta) + (\mu(\theta)|\boldsymbol{D}|^2 + s_y(\theta)|\boldsymbol{D}|). \tag{16}$$

For $|\boldsymbol{S}| < s_y(\theta)$, consistent with the requirement $\boldsymbol{D} = \boldsymbol{0}$ imposed by (10), the velocity field $\boldsymbol{v}$ must be uniform (and, thus, in particular, obey $\operatorname{div} \boldsymbol{v} = 0$), viz.,

$$\boldsymbol{v} = \text{constant}, \tag{17}$$

while the temperature θ field is determined from the heat equation

$$\varrho c \dot{\theta} = \kappa \operatorname{div}(\operatorname{grad} \theta). \tag{18}$$

The condition $|\boldsymbol{S}| = s_y(\theta)$ merely determines the boundaries between regions of viscous flow, where the governing partial differential equations are the condition of incompressibility (1), the linear momentum balance (14), and the energy balance (16), and regions of plastic flow, where the velocity field is constant and the sole partial differential equation is the heat equation (18).

3 Isothermal Case

A conventionally held belief is that lava domes exhibit a finite yield stress that controls their shape and explosivity. To explore this effect, we study an isothermal process in which an incompressible viscoplastic material spreads over a horizontal plate.

3.1 Governing Equations

Consider an incompressible Bingham thermo-visco-plastic material extruded from a point source onto a horizontal plate. Assume that, throughout this process, the temperature field remains uniform in space and time-independent, viz. $\theta = \theta_* = \text{constant}$. Define $s_* = s_p(\theta_*)$ and $\mu_* = \mu(\theta_*)$. Then, assuming that the stress power terms of the energy balance are negligible, the governing equations in the viscous zone are

$$\left.\begin{aligned} \operatorname{div} \boldsymbol{v} &= 0, \\ \varrho \dot{\boldsymbol{v}} &= -\operatorname{grad} p + \operatorname{div}\Big((\mu_* + \frac{s_*}{|\boldsymbol{D}|}) \boldsymbol{D} \Big) + \varrho \boldsymbol{g}, \end{aligned}\right\} \tag{19}$$

while the surface separating the viscous and plastic zones is determined simply by the equation

$$|\boldsymbol{S}| = s_*, \tag{20}$$

and, the governing equations in the plastic region are

$$\left.\begin{aligned} \operatorname{div} \boldsymbol{v} &= 0, \\ \varrho \dot{\boldsymbol{v}} &= -\operatorname{grad} p + \varrho \boldsymbol{g}, \end{aligned}\right\} \tag{21}$$

with the velocity field $\boldsymbol{v}$ uniform in the vertical direction. We choose cylindrical coordinates (r, ϑ, z), with origin $\boldsymbol{0}$ centered at the source of extrusion and the positive z-axis oriented vertically (opposing gravity), and we let u, v, and w denote the r, θ, and z components of $\boldsymbol{v}$.

We assume that no slip may occur at the base $z = 0$, so that

$$u(r, \vartheta, 0, t) = v(r, \vartheta, 0, t) = w(r, \vartheta, 0, t); \tag{22}$$

further, the surface $z = h(r, \vartheta, t)$ is material, whereby

$$h_t(r, \vartheta, t) + u(r, \vartheta, h(r, \vartheta, t), t)h_r(r, \vartheta, t) + \frac{1}{r}v(r, \vartheta, h(r, \vartheta, t), t)h_\vartheta(r, \vartheta, t) = w(r, \vartheta, h(r, \vartheta, t), t), \tag{23}$$

and free of traction, so that

$$\boldsymbol{T}(r, \vartheta, h(r, \vartheta, t), t)\boldsymbol{n}(r, \vartheta, t) = \boldsymbol{0}, \tag{24}$$

with

$$\boldsymbol{n}(r, \vartheta, t) = \frac{-h_r(r, \vartheta, t)\boldsymbol{e}_r + \frac{1}{r}h_\vartheta(r, \vartheta, t)\boldsymbol{e}_\vartheta + \boldsymbol{e}_z}{\sqrt{1 + h_r^2(r, \vartheta, t) + \frac{1}{r^2}h_\vartheta^2(r, \vartheta, t)}} \tag{25}$$

the outward unit normal on the dome surface.

Let H and L denote, respectively, the characteristic height and characteristic radius of the extruded layer and restrict attention to that portion of the extrusion process in which H remains small compared to L. We may then define the nondimensional parameter

$$\epsilon = \frac{H}{L} \ll 1. \tag{26}$$

Let U denote the characteristic fluid velocity in the viscous zone. We then consider a scaling with

$$r = L\tilde{r}, \qquad \vartheta = \tilde{\vartheta}, \qquad z = H\tilde{z}, \qquad t = \frac{U}{L}\tilde{t}, \tag{27}$$

and

$$\left.\begin{aligned} u(r, \vartheta, z, t) &= U\tilde{u}(\tilde{r}, \tilde{\vartheta}, \tilde{z}, \tilde{t}), \\ v(r, \vartheta, z, t) &= U\tilde{v}(\tilde{r}, \tilde{\vartheta}, \tilde{z}, \tilde{t}), \\ w(r, \vartheta, z, t) &= \epsilon U\tilde{w}(\tilde{r}, \tilde{\vartheta}, \tilde{z}, \tilde{t}), \\ p(r, \vartheta, z, t) &= \varrho g H\tilde{p}(\tilde{r}, \tilde{\vartheta}, \tilde{z}, \tilde{t}), \end{aligned}\right\} \tag{28}$$

with $g = |\boldsymbol{g}|$ the magnitude of the gravitational acceleration.

Further, we suppose that

$$U = \frac{\varrho g H^3}{\mu_*}. \tag{29}$$

Inserting the foregoing expressions in the equations (19) that hold in the viscous zone and dropping the superposed tildes on the dimensionless variables yields the dimensionless expression of the constraint of incompressibility

$$\frac{1}{r}\frac{\partial(ru)}{\partial r} + \frac{1}{r}\frac{\partial v}{\partial \vartheta} + \frac{\partial w}{\partial z} = 0 \tag{30}$$

and the dimensionless equations enforcing momentum balance

$$\left.\begin{aligned}
\epsilon^2 F^2\big(\frac{\partial u}{\partial t}+u\frac{\partial u}{\partial r}+\frac{v}{r}\frac{\partial u}{\partial \vartheta}+w\frac{\partial u}{\partial z}\big) &= -\frac{\partial p}{\partial r}+\frac{\partial S_{rz}}{\partial z}+\epsilon^2\big(\frac{\partial S_{rr}}{\partial r}+\frac{1}{r}\frac{\partial S_{r\vartheta}}{\partial \vartheta}\big),\\
\epsilon^2 F^2\big(\frac{\partial v}{\partial t}+u\frac{\partial v}{\partial r}+\frac{v}{r}\frac{\partial v}{\partial \vartheta}+w\frac{\partial v}{\partial z}\big) &= -\frac{1}{r}\frac{\partial p}{\partial \vartheta}+\frac{\partial S_{\vartheta z}}{\partial z}+\epsilon^2\big(\frac{\partial S_{r\vartheta}}{\partial r}+\frac{1}{r}\frac{\partial S_{\vartheta\vartheta}}{\partial \vartheta}\big),\\
\epsilon^2 F^2\big(\frac{\partial w}{\partial t}+u\frac{\partial w}{\partial r}+\frac{v}{r}\frac{\partial w}{\partial \vartheta}+w\frac{\partial w}{\partial z}\big) &= -\frac{\partial p}{\partial \vartheta}-1+\epsilon^2\big(\frac{\partial S_{rz}}{\partial r}+\frac{1}{r}\frac{\partial S_{\vartheta z}}{\partial \vartheta}+\frac{\partial S_{zz}}{\partial z}\big),
\end{aligned}\right\} \tag{31}$$

with

$$F=\frac{\varrho g H^{\frac{3}{2}}}{\mu_*} \tag{32}$$

the dimensionless Froude number, the components $S_{rr}, S_{r\vartheta}, S_{rz}, S_{\vartheta\vartheta}, S_{\vartheta z}$, and S_{zz} of the extra stress $\boldsymbol{S}$, are given by

$$\left.\begin{aligned}
S_{rr} &= 2\big(1+\frac{B}{E}\big)\frac{\partial u}{\partial r},\\
S_{r\vartheta} &= \big(1+\frac{B}{E}\big)\big(\frac{\partial v}{\partial r}-\frac{v}{r}+\frac{1}{r}\frac{\partial u}{\partial \vartheta}\big),\\
S_{rz} &= \big(1+\frac{B}{E}\big)\big(\frac{\partial u}{\partial z}+\epsilon^2\frac{\partial w}{\partial r}\big),\\
S_{\vartheta\vartheta} &= 2\big(1+\frac{B}{E}\big)\big(\frac{1}{r}\frac{\partial v}{\partial \vartheta}+\frac{u}{r}\big),\\
S_{\vartheta z} &= \big(1+\frac{B}{E}\big)\big(\frac{1}{r}\frac{\partial w}{\partial \vartheta}+\epsilon^2\frac{\partial w}{\partial r}\big),\\
S_{zz} &= 2\big(1+\frac{B}{E}\big)\frac{\partial w}{\partial z},
\end{aligned}\right\} \tag{33}$$

where E is defined as

$$E=\big((u_z+\epsilon^2 w_z)^2+2\epsilon^2 u_r^2+2\epsilon^2(u_r+\frac{u}{r})^2+2\epsilon^2(\frac{u}{r}+\frac{v_\vartheta}{r})^2$$

$$+(\mathrm{v}_z+\epsilon^2\tfrac{w_\vartheta}{r})^2+\epsilon^2(\tfrac{u_\vartheta}{r}+v_r-\tfrac{v}{r})^2\big)^{1/2} \tag{34}$$

and

$$B=\frac{\sqrt{2}s_* L}{\varrho g H^2} \tag{35}$$

is the dimensionless Bingham number.

We now assume that u, v, w, p and h possess regular expansions of the form

$$\left.\begin{aligned}
u &= u_0+\epsilon u_1+O(\epsilon^2),\\
v &= v_0+\epsilon v_1+O(\epsilon^2),\\
w &= w_0+\epsilon w_1+O(\epsilon^2),\\
p &= p_0+\epsilon p_1+O(\epsilon^2),\\
h &= h_0+\epsilon h_1+O(\epsilon^2),
\end{aligned}\right\} \tag{36}$$

in which case the relations (33) imply that the stress components admit regular expansions of the form

$$\left.\begin{aligned} S_{rr} &= (S_{rr})_0 + \epsilon(S_{rr})_1 + O(\epsilon^2),\\ S_{r\vartheta} &= (S_{r\vartheta})_0 + \epsilon(S_{r\vartheta})_1 + O(\epsilon^2),\\ S_{rz} &= (S_{rz})_0 + \epsilon(S_{rz})_1 + o(\epsilon^2),\\ S_{\vartheta\vartheta} &= (S_{\vartheta\vartheta})_0 + \epsilon(S_{\vartheta\vartheta})_1 + O(\epsilon^2),\\ S_{\vartheta z} &= (S_{\vartheta z})_0 + \epsilon(S_{\vartheta z})_1 + O(\epsilon^2),\\ S_{zz} &= (S_{zz})_0 + \epsilon(S_{zz})_1 + O(\epsilon^2). \end{aligned}\right\} \tag{37}$$

At leading order, equations (31) give

$$\frac{\partial p_0}{\partial r} = \frac{\partial (S_{rz})_0}{\partial z}, \qquad \frac{1}{r}\frac{\partial p_0}{\partial \vartheta} = \frac{\partial (S_{r\vartheta})_0}{\partial z}, \qquad \frac{\partial p}{\partial z} = -1. \tag{38}$$

Then, applying the boundary conditions, we obtain

$$p_0(r,\vartheta,z,t) = -(h_0(r,\vartheta,t) - z), \tag{39}$$

while $(38)_{1,2}$ yield

$$\left.\begin{aligned} (S_{rz})_0(r,\vartheta,z,t) &= -(h_0(r,\vartheta,t) - z)\frac{\partial h_0(r,\vartheta,z)}{\partial r},\\ (S_{\vartheta z})_0(r,\vartheta,z,t) &= -(h_0(r,\vartheta,t) - z)\frac{1}{r}\frac{\partial h_0(r,\vartheta,z)}{\partial \vartheta}. \end{aligned}\right\} \tag{40}$$

Alternatively, writing

$$E_0 = \sqrt{(\frac{\partial u_0}{\partial z})^2 + (\frac{\partial v_0}{\partial z})^2}, \tag{41}$$

the relations (40) can be expressed as

$$(S_{rz})_0 = \big(1 + \frac{B}{E_0}\big)\frac{\partial u_0}{\partial z}, \qquad (S_{\theta z})_0 = \big(1 + \frac{B}{E_0}\big)\frac{\partial v_0}{\partial z}. \tag{42}$$

Assume now, that the interface between viscous region and the plastic region can be represented as a surface $z = Y(r,\vartheta,t)$. The limiting value of the stress in the viscous zone must equal the yield stress, so that

$$\sqrt{(S_{rz}(r,\vartheta,t))^2 + (S_{\vartheta z}(r,\vartheta,t))^2} = B; \tag{43}$$

further, the velocity field must obey

$$\frac{\partial u_0(r,z,\vartheta,t)}{\partial z}\Big|_{z=Y(r,\vartheta,t)} = \frac{\partial u_0(r,z,\vartheta,t)}{\partial z}\Big|_{z=Y(r,\vartheta,t)} = 0, \tag{44}$$

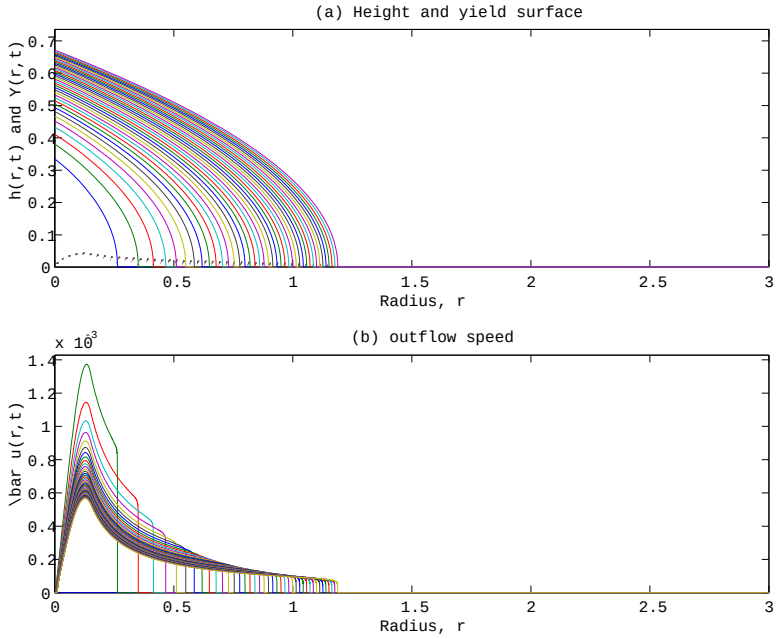

Figure 1: B = 0.1, $w_s = 0.1$, initial-value problem: $h(r, t = 0) = 0.001e^{-r/5}$

which yields

$$Y(r,\vartheta,t) = h_0(r,\vartheta,t) - \frac{B}{\sqrt{\left(\frac{\partial h_0(r,\vartheta,t)}{\partial r}\right)^2 + \frac{1}{r^2}\left(\frac{\partial h_0(r,\vartheta,t)}{\partial \vartheta}\right)^2}}. \tag{45}$$

As immediate consequences of the foregoing, we find that, for $0 \le z \le Y(r,\vartheta,t)$,

$$\left.\begin{aligned} \frac{\partial u_0(r,\vartheta,z,t)}{\partial z} &= \big(z - Y(r,\vartheta,t)\big)\frac{\partial h_0(r,\vartheta,t)}{\partial r}, \\ \frac{\partial v_0(r,\vartheta,z,t)}{\partial z} &= \big(z - Y(r,\vartheta,t)\big)\frac{1}{r}\frac{\partial h_0(r\,\vartheta,t)}{\partial \vartheta}. \end{aligned}\right\} \tag{46}$$

On the other hand, for $Y(r,\vartheta,t) \le z \le h_0(r,\vartheta,t)$, we have that

$$u_0(r,\vartheta,t) = -\frac{1}{2}h_{0r}(r,\vartheta,t)Y^2(r,\vartheta,t) \tag{47}$$

We integrate the constraint (30) of incompressibility over the vertical coordinate z from $z = 0$ to $z = h(r,\vartheta,t)$ and using (46), insert the expansions in the resulting equation, giving, to the leading order

$$\frac{\partial h_0(r,\vartheta,t)}{\partial t} + \frac{1}{r}\frac{\partial}{\partial r}\Big(r\int_0^{h_0(r,\vartheta,t)} u_0(r,\vartheta,z,t)\,dz\Big) + \frac{1}{r}\frac{\partial}{\partial \vartheta}\Big(\int_0^{h_0(r,\vartheta,t)} v_0(r,\vartheta,z,t)\,dz\Big) = w_s(r,\vartheta,t), \tag{48}$$

where $w_s(r,\vartheta,t) = w(r,\vartheta,0,t)$ is the velocity on vertical direction at $z = 0$. If the slurry is ejected from a source hole with radius r_0, then at $r = r_0$, the velocity must vanish while at $r = 0$ the velocity must attain its maximum value; here we choose w_s to both ϑ and t independent with the form:

$$w_s(r,\vartheta,t) = w_0(r - r_0)^2 \tag{49}$$

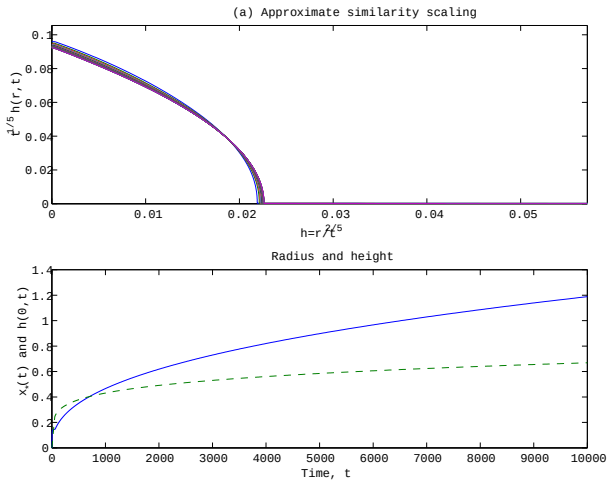

Figure 2: Same conditions as that of figure 1.

We assume also that the govering equations are independent of temperature field θ at leading order, such that $h_0 = h_0(r,t)$, $Y = Y(r,t)$, etc.

Therefore, we obtain evolution equation for the leading order height h_0 of the dome,

$$\frac{\partial h_0(r,t)}{\partial t} + \frac{1}{r}\frac{\partial}{\partial r}(r h_0(r,t)\bar{u}(r,t)) = w_s(r,t), \tag{50}$$

with

$$h_0(r,t)\bar{u}(r,t) = \Big(\int_0^{h_0(r,t)} u_0(r,z,t)\,dz\Big) = -\frac{1}{6}Y^2(r,t)\frac{\partial h_0(r,t)}{\partial r}(3h_0(r,t) - Y(r,t)), \tag{51}$$

and the height $Y(r,t)$ of yield surface being

$$Y(r,t) = h_0(r,t) + \frac{B}{\frac{\partial h_0(r,t)}{\partial r}}, \tag{52}$$

Figure 1(a) shows how h_0 evolves with time along the radial direction. The dotted line is the yield surface. Figure 1(b) shows the depth averaged velocity field along the radial direction. From Figure 2(a), an approximate similarity solution is found with $h(r,t) = r^{1/5} f(r/t^{2/5})$, which has been proposed previously[2] from the real lava field measurements and some scaling analyses.

3.2 Laboratory simulation

3.2.1 Material

Real lava is known to have a finite yield stress. The simplest substance possessing this characteristic is a slurry. Two slightly different slurries were used in these experiments. The first of these, which we call material #1, is a $1:1$ by weight mixture of kaoline and de-ionized water. The second slurry, which we call material #2 is a $1.2:1$ by weight mixture of kaoline and de-ionized water. A dial-reading viscometer (Brookfield Laboratory Viscometer company) was used to measure the yield stresses and apparent viscosities. For these slurries, which display Non-newtonian response, the measured viscosity is called the apparent viscosity. The measured material properties of these materials appear in Table 1.

Table 1

Property	Material #1 kaoline + water $1:1$ by weight	Material #2 kaoline + water $1.2:1$ by weight	Material #3 kaoline + peg 600 wax $1:1.25$ by weight
Density ϱ (g/cm^3)	1.36	1.48	1.44
Apparent viscosity η (P)	200	300	30
Yield stress s_y (dyne/cm^2)	437	2000	55
Specific heat c (J/kg×K)	–	–	1.78×10^3
Apparent viscosity η (P)	–	–	1.44×10^{-7}
Solidification temperature θ_s (K)	–	–	290

3.2.2 Experimental apparatus

Our experimental apparatus is depicted in Figure 3. The kaoline/water slurry was mixed 2 days ahead of the experiment and, once again, immediately prior to the experiment, was thoroughly mixed again using a power mixer so that no slump would occur. Operations are conducted at a room temperature of 20°C and a relative humidity of 30%. The slurry is placed in an acrylic circular cylinder 90 cm long and 11 cm in diameter. One end of the cylinder was connected via a pipe and micropump through a flow meter to a water bucket; the other end of cylinder was connected with a plastic hose (3 cm in diameter) to a horizontal aluminuum plate which has a 3 cm hole in diameter in the center. Ejection of the slurry was controlled by pumping water into the cylinder behind the piston. When filter papers were placed on the smooth aluminuum plate, there was barely any change in the flow structure, which shows that the no-slip boundary condition on the base is a valid approximation. Each run lasted between 10 and 40 minutes, depending on the flow rate and the slurry used; each run was stopped when the slurry stored in the cylinder was fully ejected.

A dome around 40 cm in diameter was obtained with each run. A CCD camera was placed 1.5 m above the top of the plate; further, a mirror placed at a 45°C angle to the edge of the plate enabled the CCD camera to include both a side-view and a top-view in the same frame. Measurements of dome radius and height were later taken from the videotapes by transfering the video frames to a computer. During this experiment, the slurry was in direct contact with air upon eruption from the source hole. Some interesting surface texture was observed during

Figure 3: Overview of the experimental apparatus

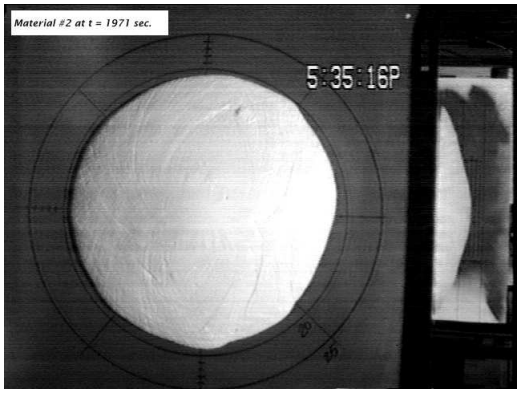

Figure 4: Snap shot of top and side view of the growing dome. note the sprial texture on the surface.

the dome growth,(cf. Figure 4). In particular, two intersecting sets of slip lines were observed. This surface texture became distinct away from the center of the dome.

3.3 Data analyis and comparison

From the measurement of the experimental data, we can find the corresponding dimensionless Bingham number and flow rate appearing in equation (52) and then, solving the resulting equation (50) numerically, we can compare the experimental data with the predications from our mathematical model. Clearly, the results from mathematical model for the isothermal problem fit very well with the experimental measurements, (cf. Figure 5). The error in Figure 5(b) is a systematic underestimate of the dome height, an underestimate, is likely due to errors in the measurement of apparent viscosity and yield stress.

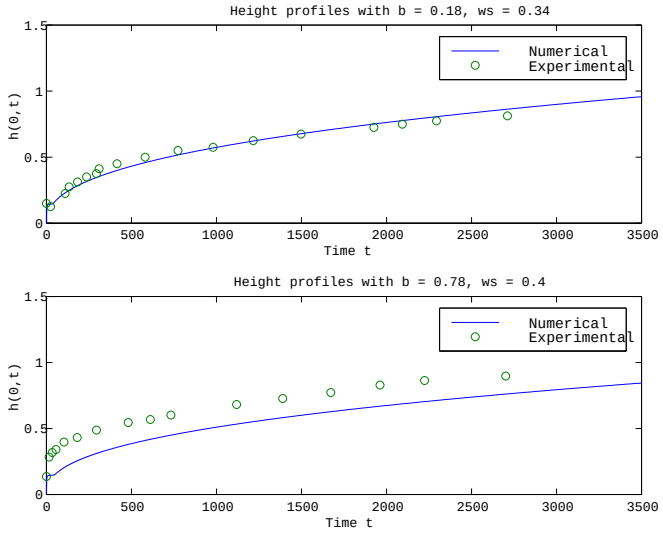

Figure 5: Comparsion of experimental data and predication from the mathematical model.

4 Thermal Effects

To account for the effect of surface cooling, we now consider the full thermo-visco-plastic model. To provide insight regarding the basic physics of dome formation with surface cooling, we first discuss the results of laboratory simulations.

4.1 Laboratory simulation

4.1.1 Material

A mixture of PEG600 wax (polyethylene glycol wax) with kaoline powder (1.25 : 1 by weight) was chosen, we call it material #3, (see table 1 for the detailed properties). PEG600 has a solidification temperature slightly lower than the room temperature and its density is greater than that of water. Further, the viscosity of material #3 is temperature dependent.

4.1.2 Apparatus

The basic setup from the isothermal experiment is retained. In addition, a $60 \times 60 \times 20$ cm acrylic box was built above the aluminium plate. During the experiment, this box was filled with circulating cold water the temperature of which was controlled by the refrigating bath system. Before and after each run, the injection hole was plugged from above to separate the slurry from the cold water. The shape and surface texure of the dome under cooling displayed dependence on the ambient water temperature and the flow rate of the slurry. When the ambient water temperature was higher than 10°C, the extruded slurry grew symmetrically throughout the experiment, except that some rims of small fingers developed at the flow

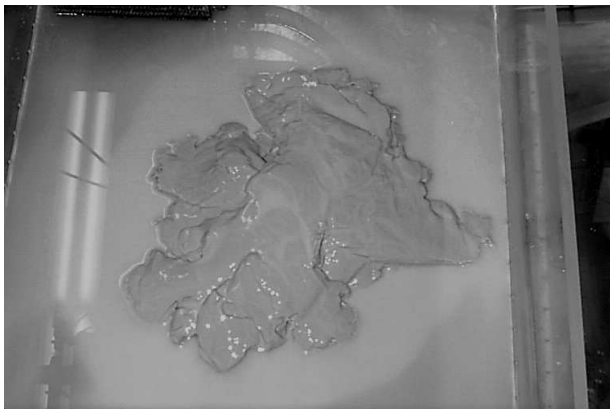

Figure 6: Snap shot after slurry is ejected into an ambient water bathing at temperature $7.5^\circ C$

front. In particular, when the ambient water temperature was lower than 10°C, Further, the surface cooled immediately once the slurry was ejected from the source and the dome structure became asymmetric with three to six lobes developing (cf. Figure 6). Clearly the shape and morphology of the dome is much more complicated in the presence of surface cooling, which reflects more closely the circumstances prevailing during the growth of real lava domes.

4.2 Governing Equations

With thermal effects included, (30) and (31) remain valid, however, the relation (33) determining the stress components become temperature dependent. Recall that for $|\boldsymbol{S}| > s_y(\theta)$, the choice (10) implies that

$$\boldsymbol{S} = \big(\mu(\theta) + \frac{s_y(\theta)}{|\boldsymbol{D}|}\big)\boldsymbol{D}. \tag{53}$$

Here, we assume that the reciprocal mobility has the spedific form

$$\mu(\theta) = \mu_* e^{-\gamma(\theta-\theta_0)} \tag{54}$$

and that the yield stress is constant, viz.,

$$s(\theta) = s_* \tag{55}$$

Consider, now, the energy balance (16) with the boundary conditions:

$$\theta_z(r,\vartheta,0,t) = 0, \qquad \kappa\,\theta_z(r,\vartheta,h(r,\vartheta,t),t) = -\alpha\,(\theta(r,\vartheta,h(r,\vartheta,t),t) - \theta_0) \tag{56}$$

Where α is the cooling rate. Substitute (54) and (55) into the energy balance equation (16), and non-dimensionalizing using the same scaling in equation (3.9)-(3.11) of the isothermal problem, we arrive at the non-dimensional form:

$$\dot\theta = \frac{\kappa}{\varrho c}\,\mathrm{div}\,(\mathrm{grad}\,\theta) + \frac{\mu_* UL}{\varrho c H^2 \theta_*} e^{-\gamma(\theta-\theta_0)}(\mu u_z^2 + \mathcal{B} u_z) \tag{57}$$

where θ_* is the characteristic temperature. The second term on the right hand side of (57) is of order $O(\epsilon)$. This indicates that the heat generated by the viscous force is very small. Further, assuming that governing equations are independent of ϑ, we have

$$\dot{\theta} = \bar{\kappa}\theta_{zz} + \frac{\bar{\kappa}}{r}\frac{\partial}{\partial r}(r\theta_r), \tag{58}$$

with $\bar{\kappa}$ the dimensionless diffusivity. We introduce the depth averaged temperature field $\bar{\theta}$ through

$$h(r,t)\bar{\theta}(r,t) = \Big(\int_0^{h(r,t)} \theta(r,t)\, dz\Big). \tag{59}$$

We integrate (58) over the vertical coordinate z from $z = 0$ to $z = h(r,t)$ and apply the boundary conditions to find, that after dropping bars,

$$h\theta_t = -w_s(\theta - \theta_v) - \theta\alpha - h\bar{u}\theta_r + \frac{\kappa}{r}\frac{\partial}{\partial r}(rh\theta_r) \tag{60}$$

where θ_v is the temperature of the slurry at the vent. Furthermore, the height evolution equation can be derived as in the isothermal case, the only differnece being due to the temperature dependence of the viscosity.

$$\left.\begin{aligned} h_t &= w_s - \frac{1}{r}\frac{\partial(rh\bar{u})}{\partial r}, \\ h\bar{u} &= -\frac{1}{6}y^2(3h - y)h_r e^{\gamma(\theta-\theta_0)}, \end{aligned}\right\} \tag{61}$$

As before,

$$y(r,t) = h_0(r,t) + \frac{B}{\frac{\partial h_0(r,t)}{\partial r}}, \tag{62}$$

The coupled system of two partial differential equations consisiting of (60) and (61) was solved numerically. There are two noteworthy limiting cases of the governing equations (60) and (61). If the cooling rate is small, i.e. $\alpha = 10^{-4}$, the temperature field θ is approximately the vent temperature θ_v. Once the slurry moves past the source, the convection term $h\bar{u}\theta_r$ is balanced by the cooling term $\alpha\theta$, therefore, we have:

$$\left.\begin{aligned} \theta &\to \theta_v \qquad \text{as} \qquad r \le r_0 \\ \bar{u}\theta_r &\to -\frac{\alpha\theta}{h} \qquad \text{as} \qquad r \ge r_0 \end{aligned}\right\} \tag{63}$$

Since the diffusitivity is very small in this case, the temperature field will eventually reach a steady state after enough time steps. It is found that the temperature field does affect the shape of the dome height, (cf.Figure 7).

The other interesting limiting case is when the cooling rate is considerably larger, i.e $\alpha = 10^{-1}$. From (60), the cooling term is approximately balanced with the source term because h and $\bar{u}$ are both small. Therefore, from (60), we have

$$\theta = \frac{w_s\theta_0}{\alpha + w_s}, \tag{64}$$

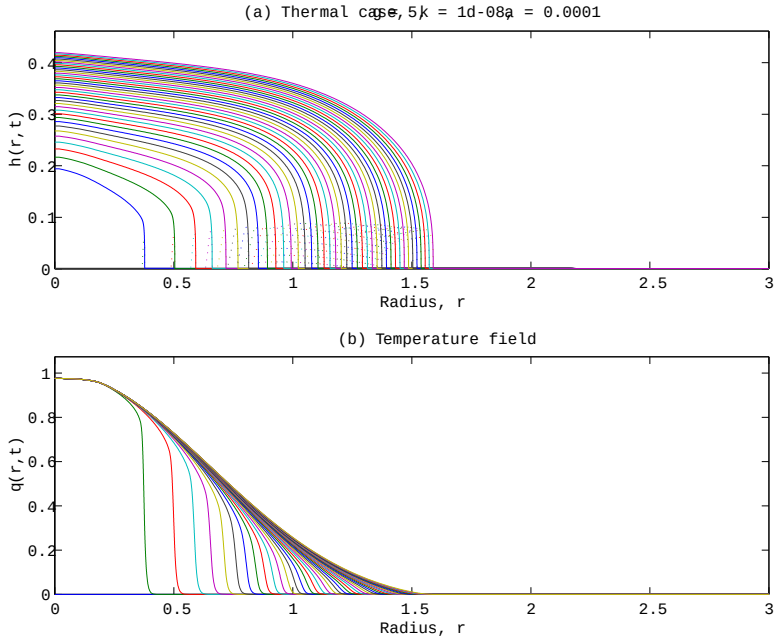

Figure 7: Height and termperature field with smaller cooling rate.

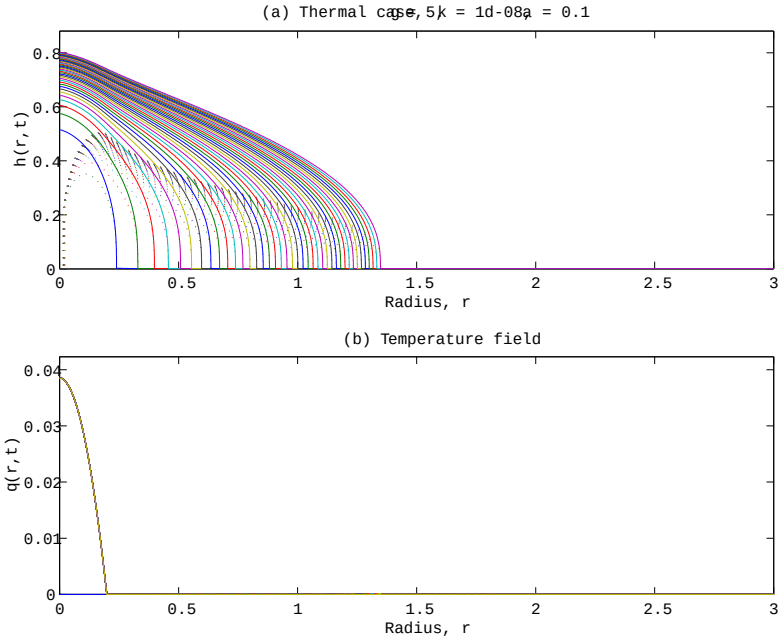

Figure 8: Height and termperature field with larger cooling rate.

where $w_s = w_0(r - r_0)^2$,

$$\left.\begin{array}{rll} \theta \to \theta_v & \text{as} & r \le r_0 \\ \theta \to 0 & \text{as} & r \ge r_0 \end{array}\right\} \tag{65}$$

Comparing Figures 7 and 8, the only parameter changes is the cooling rate. For higher cooling rates, the height of the dome grows more slowly; meanwhile, the dome grows more rapidly along the radial direction. This explains some aspects of what is observed in the thermal experiments.

5 Conclusion and future work

We formulated a continuum model. From our isothermal study, it was found that results from this model agree fairly well with those obtained from experimental simulations. The modeling is sucessful in several aspects. First of all, granted an accurate measurement of the viscosity and yield stress of the material, the height evolution equation (3.32) gives a very good predication for the dome growth during the isothermal experiment. Secondly, an approximate similarity solution for equation (3.32) was found, a solution that compares well with the previous field measurements and experimental data.

For the thermal problem, a simplified model was proposed that enables us to explain qualatively of the relation between cooling rate and the dome growth. Two limiting cases were considered and studied numerically, showing that with larger cooling rate, the dome grows more slowly in the vertical direction, which is consistent with what we have observed in our experiments. On the other hand, for the real lava dome, the diffusivity is rather small. Therefore the diffusion term in the energy equation should be neglected; Within the molten lava, initially, the temperature will be constant everywhere, but once the lava surface cools, a thin thermal boundary layer will initially form and travel from the surface to the molten part of lava. Originally, this layer is very thin and lies in the plug region. Consider the energy balance equation (16). No depth averaged fields were used here. Since κ is small, both the diffusion term and the heat generated by the viscous force term are negligible at leading order and equation (16) becomes $\dot{\theta} = 0$. At this stage, the thermal boundary layer is so thin that the velocity in this layer equals the plug velocity which is negligible; therefore, the temperature field remains constant and the growth of lava domes will not be effected by this thin thermal boundary layer. When the thermal boundary layer becomes thicker, especially when its thickness gets close to or exceeds the thickness of the plug region, the temperature field in the entire domain will be substantially changed and the viscosity and yield stress will also change. The velocity field will then be effected, since the flow is controlled by coupled partial differential equations (1), (14), (16) deduced from the mass, momentum and energy balances. The dome growth will become very complicated. Since, under this circumstance, it is very difficult to model the problem, further studies are needed.

For the thermal experiment, nonaxisymmetry is observed when surface begins to cool. Physically, we can explain this as followings. Since the dome is initially symmetric when the slurry is ejected from the source onto a horizontal surface, given a small perturbation to the height, the dome height of some portions will be increased while that of others will be decresed;

for those portions with increased height, the cooling rate becomes smaller compared with that of the initial state; material then becomes more viscous and this portion of the material can flow out easily; meanwhile, in the portions with decreased height, the cooling rate becomes larger which makes the material less viscous and more plastic like, hence this poriton is in stead dammed-up. That's how nonaxisymmetric structure eventually develop.

Also, realistically, surface cooling and solidification are both important factors in the flow morphology. If "lobes" observed in the thermal experiment are caused by the solidification of the material, we assume that they are very superficial and fragmented; hence the associated forces are small, thereafter, solidification factor is not considered here.

Instability analyis and flow morphology studies will be the direction for the future work.

6 Acknowledgements

I would like especially thank Neil Balmforth for introducing this project to me and for helpful discussions, encouragement throughout the summer; I also owe thanks to Bill Young and Richard Craster for interesting discussions, to Jack Whitehead for letting me use his wonderful lab, and to John Salzig for building the laboratory apparatus for me—without him, my experiments would have been impossible. Thanks also go to Jeff Parsons lending me a viscometer from MIT and to George Veronis, to Joe Keller for teaching me the basic lessons in softball, and to the Maury Lane residents for all the fun and food we shared. Finally, thanks to all the GFD staff and fellows, whose company made for a great summer.

References

[1] G. Hulme, "The interpretation of lava flow morphology," Geophys. J. R. astr. Soc. **39**, 361 (1974).

[2] S. Blake, "Viscoplastic models of lava domes," in IAVCEI Proceedings in Volcanology, Vol.2, edited by J. Fink (Springer-Verlag, 1989).

[3] C. R. J. Kilburn, "General patterns of flow field growth: Aa and blocky lavas ," Journal of Geophysical Research, **96**, 19,721 (1991)

[4] M. Dragoni, S. Pondrelli & A. Tallarico, "Longitudinal deformatioon of a lava flow: the influence of Bingham rheology," Journal of Volcanology Geothermal Research, **52**, 247 (1992)

[5] J. Fink & R. Griffiths, " A laboratory analog study of the surface morphology of lava flows extruded from point and line sources," Journal of Volcanology Geothermal Research, **54**, 19 (1992)

[6] M. V. Stasiuk, C. Jaupart & R. S. Sparks, "Influence of cooling on lava-flow dynamics," Geology, **21**, 335 (1993)

[7] R. Griffiths & J. Fink, "Effects of surface cooling on the spreading of lava flows and domes," J. Fluid. Mech., **255**, 667 (1993)

[8] R. Griffiths & J. Fink, "Solidifying Bingham extusions: a model for the growth of silicic lava domes," J. Fluid. Mech., **347**, 13 (1997)

[9] J. Fink & R. Griffiths, "Morphology, eruption rates, and rheology of lava domes: Insights from laboratory models," Journal of Geophysical Research, **96**, 19,721 (1991)